arXiv:1110.2232v2 [quant-ph] 16 Apr 2012

Quantum Circuit Design for Solving Linear Systems of Equations

Yudong Cao,[1] Anmer Daskin,[2] Steven Frankel,[1] and Sabre Kais[3,*]

[1]*Department of Mechanical Engineering, Purdue University*
[2]*Department of Computer Science, Purdue University*
[3]*Department of Chemistry, Physics and Birck Nanotechnology Center, Purdue University, West Lafayette, IN 47907 USA*

Recently, it has been demonstrated that quantum computers can be used for solving linear systems of algebraic equations with exponential speedup compared with classical computers. Here, we present an efficient and generic quantum circuit design for implementing the algorithm for solving linear systems. In particular, we show the detailed construction of a quantum circuit which solves a 4×4 linear system with 7 qubits. It consists of only the basic quantum gates that can be realized with present physical devices, implying great possibility for experimental implementation. Furthermore, the performance of the circuit is numerically simulated and its ability to solve the intended linear system is verified.

Quantum computers are devices that take direct advantage of quantum mechanical phenomena such as superposition and entanglement to perform computations [1]. Because they compute in ways that classical computers cannot, for certain problems quantum algorithms provide exponential speedups over their classical counterparts. For example, in solving problems related to factoring large numbers [2] and simulation of quantum systems [3–17], quantum algorithms are able to find the answer exponentially faster than classical algorithms. Recently, A. W. Harrow, A. Hassidim and S. Lloyd [18] proposed a quantum algorithm for solving linear systems of equations with exponential speedup over the best known classical algorithms.

With the theoretical potential of the algorithm, an equally important issue is to render the algorithm viable for experimental implementation. Therefore, in this work we present a generic quantum circuit design based on the theoretical framework outlined by the algorithm. Particularly, the original work [18] did not elaborate on the circuit design for implementing λ_j^{-1}-controlled rotation when only λ_j is available. Hence in this work we present a scalable design of the quantum circuit for finding the reciprocals of the eigenvalues λ_j and stored them in a quantum register with a superposition of states that encode the values of λ_j^{-1} in binary format. The runtime scaling of this inverting circuit is $O(\log N)$, which retains the advantageous $O(\log N)$ runtime for the overall algorithm. For the purpose of showing a concrete numerical example of how this scheme works, we choose a specific linear system (described by a matrix A of dimension 4×4) as the numerical example for of the algorithm. Since our circuit involves only 7 qubits and is composed of only basic quantum gates, our work bridges the theoretical development of the algorithm with the possibility of physical implementation by experimentalists.

The algorithm[18] solves the problem $A\vec{x}=\vec{b}$ where A, a Hermitian d-sparse $N\times N$ matrix and $\vec{b}$, a unit vector are given. The major steps of the algorithm can be summarized as the following: (1) Represent the vector $\vec{b}$ as a quantum state $|b\rangle=\sum_{i=1}^{N}b_i|i\rangle$ stored in a quantum register (termed B), where $|i\rangle$ represents a basis state of the register B where the states of the qubits represent the binary coding of i. In a separate quantum register (termed C) of t qubits, initialize the qubits by transforming the register to state $\sum_\tau|\tau\rangle$ from $|0\rangle$. Here $|\tau\rangle$ represents a basis state of the register C where the states of the qubits represent the binary coding of τ; (2) Apply the conditional Hamiltonian evolution $\sum_{\tau=0}^{T-1}|\tau\rangle\langle\tau|^C\otimes e^{iA\tau t_0/T}$; (3) Apply the quantum inverse Fourier transform to the

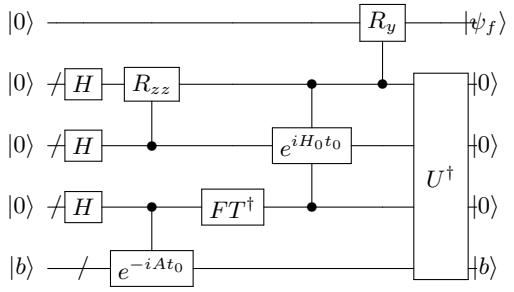

FIG. 1: Overall circuit design. The registers from top to bottom are respectively the ancillary qubit, register L, M, C and B. The initial state is denoted as $|0000b\rangle$. $|\psi_f\rangle = \sqrt{1-\frac{C^2}{\lambda_j^2}}|0\rangle + \frac{C}{\lambda_j}|1\rangle$. $U^\dagger$ represents uncomputation.

register C. Denote the basis states after quantum Fourier transform as $|k\rangle$. At this stage, the amplitudes of the basis states are concentrated on k values that satisfy $\lambda_k \approx \frac{2\pi k}{t_0}$, where λ_k is the k-th eigenvalue of the matrix A; (4) Add an ancilla qubit and apply conditional rotation on it, controlled by the register C with $|k\rangle \approx |\lambda_k\rangle$. The rotation tranforms the qubit to $\sqrt{1-\frac{C^2}{\lambda_j^2}}|0\rangle + \frac{C}{\lambda_j}|1\rangle$. This is a key step of the algorithm and it involves finding the reciprocal of the eigenvalue λ_j quantum mechanically, which is not a trivial task on its own. We will elaborate on how to achieve this later in this work; (5) Uncompute the registers b and C, and (6) Measure the ancilla bit. If it returns 1, the register b of the system is in the state $\sum_{j=1}^{n} \beta_j {\lambda_j}^{-1}|u_j\rangle$ up to a normalization factor, which is equal to the solution $|x\rangle$ of the linear system $A\vec{x} = \vec{b}$. Here $|u_j\rangle$ represents the j-th eigenvector of the matrix A and let $|b\rangle = \sum_{i=1}^{n} \beta_j |u_j\rangle$.

Based on the theoretical framework of the algorithm outlined above, here we present a generic quantum circuit design that implements the algorithm to find the solution $|x\rangle$ to the linear equation $A|x\rangle = |b\rangle$. The circuit contains registers B, C, M, L and an ancillary qubit (Figure 1). The detailed matrix forms of the quantum gates are presented in Appendix.

Here the time parameter t_0 for all Hamiltonian simulations is defined to be 2π. Register B is used to store the value of $|b\rangle$. Register C, M and L contain t, m and l qubits respectively. the Walsh-Hadamard transform on Register C, the controlled Hamiltonian simulation and the inverse Fourier transform ideally gives a state $\sum_j \beta_j |\lambda_j\rangle|u_j\rangle$ [18] in Register B and C. At the same time, Walsh-Hadamard transform and controlled global phase shift R_{zz} is applied to register L and M (Figure 1) and the state of the two registers becomes $\sum_p \sum_s \exp(i\frac{p}{2^m}t_0)|s\rangle|p\rangle$, where $|p\rangle$ and $|s\rangle$ represent the basis states of the register M and L respectively. Details of this part of the circuit is shown in Figure 5. After the inverse Fourier transform is executed on register C, we use its $|\lambda_j\rangle$ states stored in register C as a control for a Hamiltonian simulation $\exp(iH_0t_0)$ that is applied on register M (Details in Figure 6). Here H_0 is defined as diagonal matrix whose diagonal elements are $(1, 2, ..., 2^{m-1})$. Due to the unitary nature of $\exp(iH_0t_0)$, the operation $\exp(iH_0t_0)$ can be readily decomposed into a quantum circuit [19, 20] that consists of only basic quantum gates.

We further establish the control relationship between Register L and the $\exp(iH_0t_0)$ by using the the k_l-th qubit (Figure 6) of the register L to control a $\exp[-ip(\frac{\lambda_j}{2^m}\frac{1}{2^{l-k_l}}t_0)]$ simulation that acts on register M. The values of binary numbers stored in register L are then able to determine the time parameter t in the overall Hamiltonian simulation $\exp(-iH_0t)$. Following such construction, after the Hamiltonian simulation $\exp(-iH_0t_0)$ the state of the system is $|0\rangle \otimes \sum_{j=1}^{n} \sum_{p=0}^{2^m-1} \sum_{s=0}^{2^l-1} \beta_j \exp[i\frac{p}{2^{m+l}}t_0 (2^l - \lambda_j s)] |s\rangle|p\rangle |\lambda_j\rangle|u_j\rangle$. With $t_0 = 2\pi$, the states $|s\rangle$ is concentrated on values of $s = \frac{2^l}{\lambda_j}$ in the above expression (Denote such $|s\rangle$ states as $|\frac{2^l}{\lambda_j}\rangle$). This is because of the fact that sums of the form $\sum_{k=0}^{N-1} \exp(2\pi i k\frac{r}{N})$ vanish unless $r = 0 \mathrm{mod} N$. Denote the components of the superposition states in register L as $|\frac{2^l}{\lambda_j}\rangle$. Ro-

tate the ancilla bit with the angle shift controlled by the $|\frac{2^t}{\lambda_j}\rangle$ states stored in register L: $R_y(\frac{2^t}{\lambda_j})|0\rangle \approx \sqrt{1-\frac{C^2}{\lambda_j^2}}|0\rangle + \frac{C}{\lambda_j}|1\rangle$ with C being a constant. Uncomputing the three registers (Figure 1), we are left with a state in register B with the ancilla qubit proportional to $\sum_{j=1}^{n}\left[\sqrt{1-C^2/\lambda_j^2}|0\rangle + C/\lambda_j|1\rangle\right] \otimes |000\rangle \otimes \beta_j|u_j\rangle$

Measuring the ancilla qubit and if we obtain $|1\rangle$, the state of the system will collapse to $|1000\rangle \otimes \sum_{j=1}^{n}\beta_j\lambda_j^{-1}|u_j\rangle$, where $|u_j\rangle$, where the first register represents the solution. If the ancilla bit measures $|0\rangle$, the system is back to its original state $|0000b\rangle$. If the ancilla bit measures $|1\rangle$, the state stored in the register B is proportional to the solution of the linear system of equations $A|x\rangle = |b\rangle$ and the register B is no longer entangled with any other registers in the system. Therefore we have obtained the solution of the linear system of equations in form of a quantum superposition state stored in the register B.

There are mainly two factors that influence the number of qubits needed in register L and M. The first one is the desired bit precision for encoding both λ_j and $\frac{1}{\lambda_j}$. Clearly if one desires to encode a number with precision $\epsilon = O(2^q)$, at least q qubits are needed for the register, which is true for any generic binary registers. In addition to this factor, for the particular roles that the register L and M play in the circuit, the condition number κ of A and the condition number of the matrix A is also important. Because in order for the inversion circuit to work, 2^m must be larger than any eigenvalue of A i.e. $m \geq \lceil \log \lambda_{max} \rceil$. On the other hand in order to encode all values of $\frac{1}{\lambda_j}$ register L must have enough qubits such that even the largest one $\frac{1}{\lambda_{min}}$ can be encoded i.e. $l \geq \lceil \log \lambda_{min} \rceil$. Therefore $m - l \approx \log \kappa$ is a general constraint that m and l must comply with.

A detailed runtime analysis in [18] shows that the runtime scales as $O(\log(N)d^2)$ where d is the sparsity of A. The circuit that we present

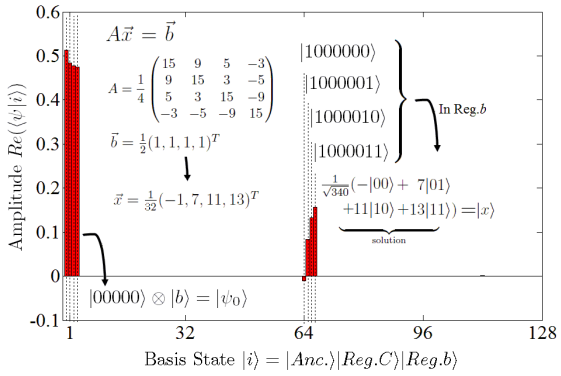

FIG. 2: The final state of the algorithm for solving the 4×4 system. The horizontal axis represents the decimal value that corresponds to a basis state of the seven-qubit system. The vertical axis represents the real parts of the probability amplitudes that corresponds to a certain basis.

here adds to the algorithm the additional complexity of controlled Hamiltonian simulation $\exp(iH_0t_0)$. However, it is shown in [21] that e^{iAt} can be simulated in time $O(\log(N)d^2t)$. Therefore the Hamiltonian simulations in this circuit design only add at most a constant overhead to the cost scaling of the algorithm.

With the generic circuit model outlined above, now we present a 7-qubit circuit for solving a system with A of dimension 4×4 as a numerical example. For the numerical example we specifically choose the form of matrix A such that it allows for a very simple *ad hoc* design of the circuit for finding the reciprocal modulo 2^t (in the 7-qubit case $2^t = 16$). For this example we choose

$$A = \frac{1}{4}\begin{pmatrix} 15 & 9 & 5 & -3 \\ 9 & 15 & 3 & -5 \\ 5 & 3 & 15 & -9 \\ -3 & -5 & -9 & 15 \end{pmatrix} \quad (1)$$

Hence A is a Hermitian matrix with the eigenvalues $\lambda_i = 2^{i-1}$ and corresponding eigenvec-

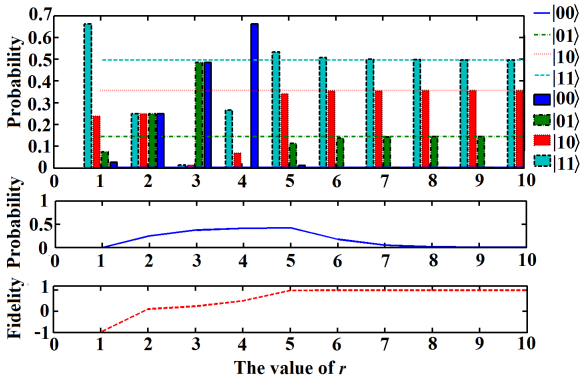

FIG. 3: Simulation results on the dependence of final state on the value of the parameter r. The first barplot shows the probability distributions over the four basis states of Register M with different values of r in the controlled rotation gates acted upon the ancilla bit. The horizontal dashed lines show the analytical values of the probabilities. The two plots following show the probability of getting the solution as well as the fidelity $\langle x'|x\rangle$ as functions of r.

tor $|u_i\rangle = \frac{1}{2}\sum_{j=1}^{4}(-1)^{\delta_{ij}}|j\rangle^C$, where $|j\rangle^C$ represents the state of register C which encode the number j in binary form, δ_{ij} is the Kronecker delta, and the index i runs from 1 to 4. Furthermore, we let $\vec{b} = \frac{1}{2}(1,1,1,1)^T$. Therefore, $|b\rangle = \sum_{j=1}^{4}\beta_j|u_j\rangle$ and each $\beta_j = \frac{1}{2}$. To compute the reciprocals of the eigenvalues, a quantum *swap* gates is used (Figure 4) to exchange the values of the first and third qubit. Therefore there is no need for specific auxiliary registers M and L (Figure 1) in this example. The eigenvalues are inverted to their reciprocals with the *swap* gate in the following fashion. For example, the eigenvalue λ_4 =8 is encoded as $|1000\rangle$ in register C, after applying the *swap* gates it is transformed to $|0010\rangle$, which is equal to $\frac{1}{8}\times 2^4 = 2$.

Figure 4 shows the circuit. We use Group Leader Optimization Algorithm to find the circuit decomposition of the Hamiltonian simulation operator $e^{iA\frac{2\pi}{16}}$ (see [19, 20] for details, also see [1, 22] for general methods). Here we let $t_0 = 2\pi$. The resulting quantum circuit for $e^{iA\frac{2\pi}{16}}$ is shown in Figure 4. With the decomposition of $e^{iA\frac{2\pi}{16}}$ readily available, the operators $e^{iA\frac{2\pi}{8}}$, $e^{iA\frac{2\pi}{4}}$ and $e^{iA\frac{2\pi}{2}}$ can be implemented by simply multiplying the angle shifts in all the rotation gates in the circuit for $e^{iA\frac{2\pi}{16}}$ by a factor of 2, 4, and 8 respectively [19].

The final state of system, conditioned on obtaining $|1\rangle$ in the ancilla bit, is $\frac{1}{\sqrt{85}}(8|u_1\rangle + 4|u_2\rangle + 2|u_3\rangle + |u_4\rangle)\otimes|0000\rangle\otimes|1\rangle$. Written in the standard bases, it becomes $\frac{1}{\sqrt{340}}(-|00\rangle + 7|01\rangle + 11|10\rangle + 13|11\rangle)$, which is proportional to the exact solution of the system $\vec{x} = \frac{1}{32}(-1,7,11,13)^T$ (Figure 2). The quantum circuits (Figure 4) outlined above is then simulated and the statistics of final states that are computed from the simulations (Figure 3).

The exponent r in the rotation gates $R(\frac{n\pi}{2^{r-1}})$ (Figure 4) is an important parameter that determines the accuracy of the final state of the system, which contains the solution to the linear system of equations. As can be seen in Figure 3, when the value of r is sufficiently large, say larger than 6, the probabilities of measuring each basis state $|00\rangle$, $|01\rangle$, $|10\rangle$ and $|11\rangle$ converge to the analytical values. Those analytical values correspond to the analytical solution of the 4×4 system $\vec{x} = \frac{1}{64}(-1,7,11,13)^T$. Furthermore, the fidelity of the results $\langle x'|x\rangle$ increases as r is increased. However, in Figure 3, as r grows beyond around 5, the probability of measuring the ancilla bit as $|1\rangle$ decays, which indicates that as r is increased, the solutions obtained in the final state in register b becomes more accurate yet less probable to attain.

In conclusion, in this work we present constructions of quantum circuits, both general and particular, for implementing the algorithm for solving linear systems of equations. Our results may motivate experimentalists with the capability of addressing 7 or more qubits and execute basic quantum gates on their setups to implement the algorithm and verify its results. Future work regarding the improvement upon

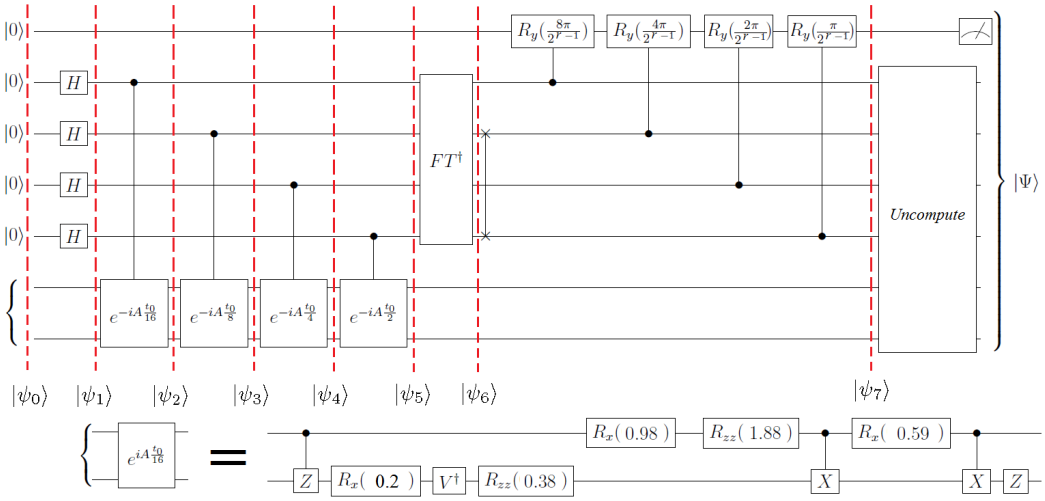

FIG. 4: Quantum Circuit for solving $A\vec{x} = \vec{b}$ with $A_{4\times4}$ being the matrix shown in equation (1). The first qubit at the top of the figure is the ancilla bit. The four qubits in the middle stand for the register C. The two qubits at the bottom is the register that stores the vector $\vec{b}$. The detailed matrix forms of the quantum gates are presented in Appendix.

the algorithm needs to be focused on topics such as extending the algorithm to cases where the matrix A has a high condition number [23].

ACKNOWLEDGMENT

This work is dedicated to professor Dudley Herschbach in appreciation of his contribution to science and celebration of his 80th birthday. Also we thank the NSF Center for Quantum Information and Computation for Chemistry, Award number CHE-1037992.

APPENDIX

The matrix representations of the quantum gates and algorithms used in this work are the following: X, Y and Z gates which are the Pauli operators σ_x, σ_y and σ_z and Hadamard gate:

$$X = \begin{pmatrix} 0 & 1 \\ 1 & 0 \end{pmatrix}, Y = \begin{pmatrix} 0 & -i \\ i & 0 \end{pmatrix} \quad (2)$$

$$Z = \begin{pmatrix} 1 & 0 \\ 0 & -1 \end{pmatrix}, H = \frac{1}{\sqrt{2}} \begin{pmatrix} 1 & 1 \\ 1 & -1 \end{pmatrix} \quad (3)$$

S gate and T gate (or $\frac{8}{\pi}$) gate are

$$S = \begin{pmatrix} 1 & 0 \\ 0 & i \end{pmatrix} T = \begin{pmatrix} 1 & 0 \\ 0 & \exp(i\frac{\pi}{4}) \end{pmatrix} \quad (4)$$

Square root of X gate (or NOT gate) and its conjugate are

$$V = \frac{1}{2} \begin{pmatrix} 1+i & 1-i \\ 1-i & 1+i \end{pmatrix}, V^\dagger = \frac{1}{2} \begin{pmatrix} 1-i & 1+i \\ 1+i & 1-i \end{pmatrix} \quad (5)$$

Rotation gates are

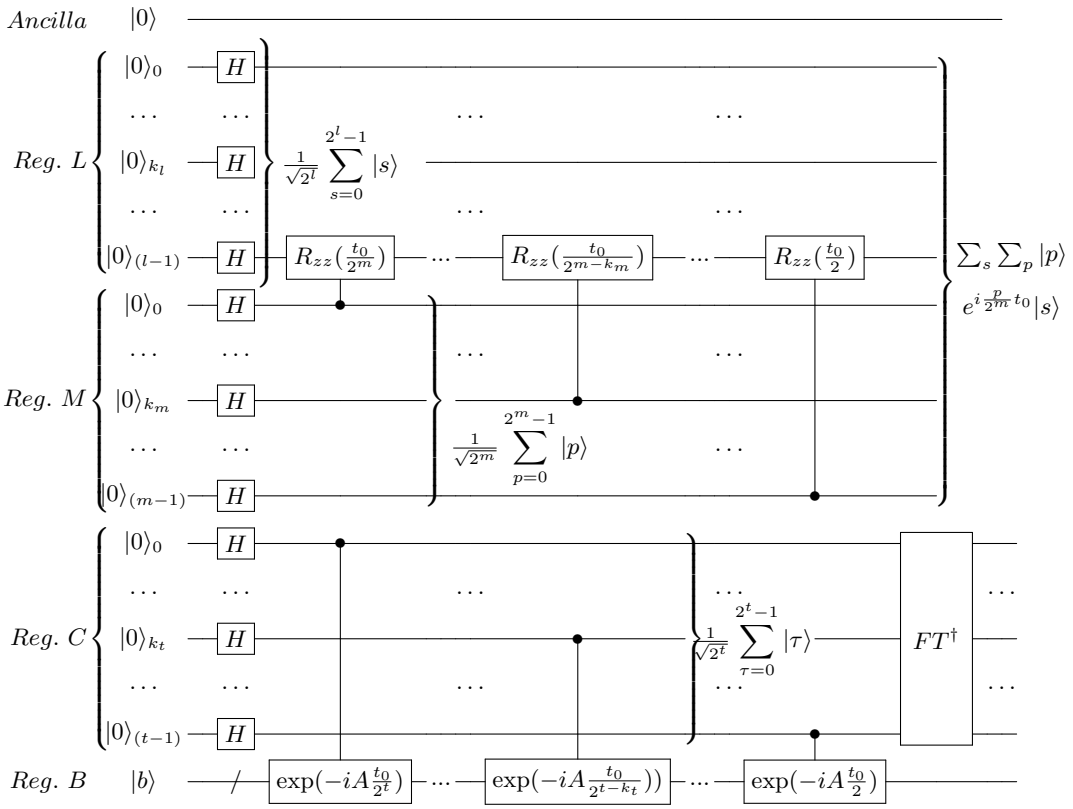

FIG. 5: Detailed quantum circuit of the generic circuit implementation. This figure shows the Walsh-Hadamard transform, $|\tau\rangle$-controlled Hamiltonian simulation e^{iAt} and Fourier transform on the register C.

$$R_x(\theta) = \begin{pmatrix} \cos(\frac{\theta}{2}) & i\sin(\frac{\theta}{2}) \\ i\sin(\frac{\theta}{2}) & \cos(\frac{\theta}{2}) \end{pmatrix} \quad (6)$$

$$R_y(\theta) = \begin{pmatrix} \cos(\frac{\theta}{2}) & \sin(\frac{\theta}{2}) \\ -\sin(\frac{\theta}{2}) & \cos(\frac{\theta}{2}) \end{pmatrix} \quad (7)$$

$$R_z(\theta) = \begin{pmatrix} 1 & 0 \\ 0 & \exp(i\theta) \end{pmatrix} \quad (8)$$

$$R_{zz}(\theta) = \begin{pmatrix} \exp(i\theta) & 0 \\ 0 & \exp(i\theta) \end{pmatrix} \quad (9)$$

BIBLIOGRAPHY

* Corresponding author:kais@purdue.edu

[1] M. A. Nielsen and I. L. Chuang, *Quantum Computation and Quantum Information* (Cambridge University Press, Cambridge, United Kingdom, 2000).

[2] P.W.Shor, in *Proc. 35th Annu. Symp. Found. Comp. Sci.*, edited by S.Goldwasser (IEEE Computer Society Press, New York, 1994) pp. 124–134.

[3] S. Lloyd, Science **273**, 1073 (1996).

[4] D. S. Abrams and S. Lloyd, Phys. Rev. Lett. **83**, 5162 (1999).

[5] D. S. Abrams and S. Lloyd, Phys. Rev. Lett. **79**, 2586 (1997).

[6] A. Papageorgiou, I. Petras, J. F. Traub, and C. Zhang, (arXiv:1008.4294v2).

[7] A. Papageorgiou and C. Zhang, (arXiv:1005.1318v3).

[8] H. Wang, S. Kais, A. Aspuru-Guzik, and M. R.

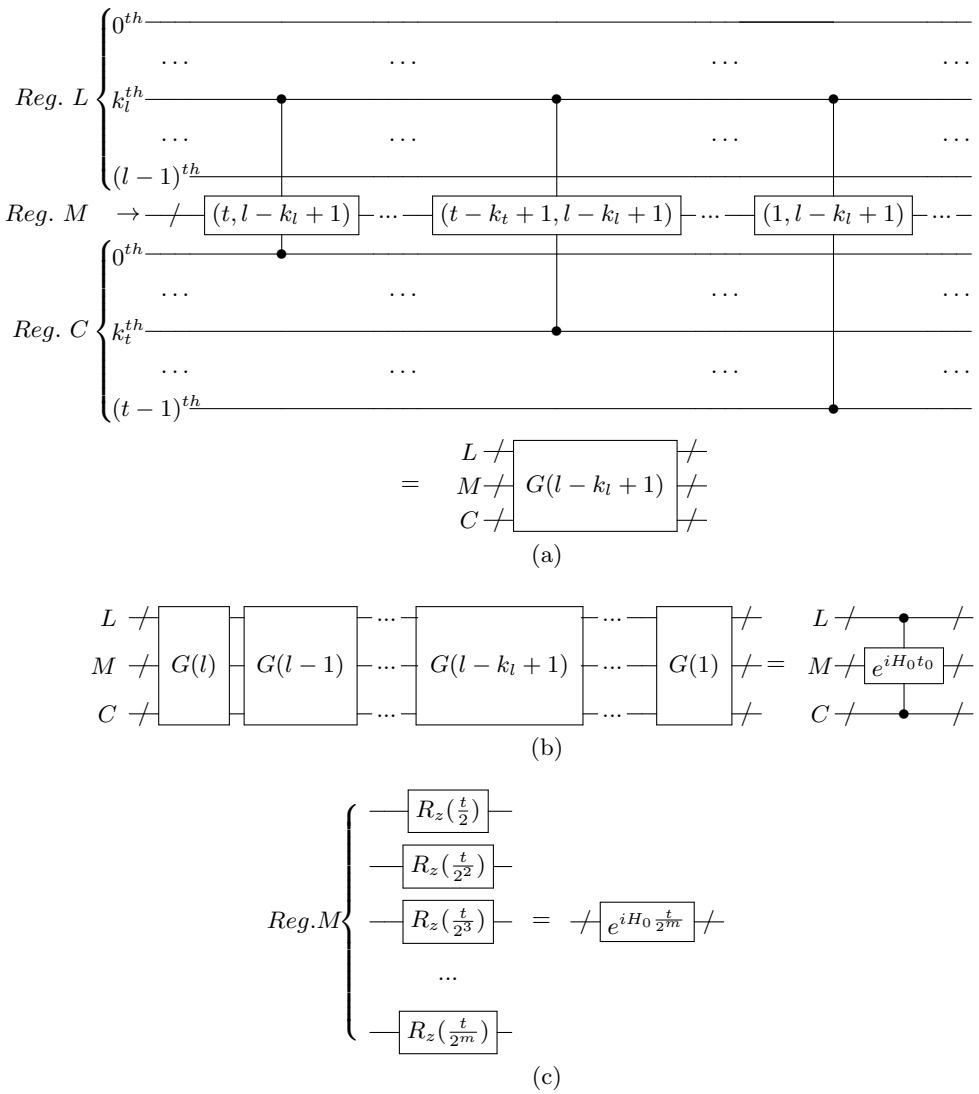

FIG. 6: Hamiltonian Simulation e^{iH_0t} which is controlled by reigster L and C. (a) A subroutine of the Hamiltonian simulation of the matrix H_0. Every gate labelled (u, v) in this diagram represents a quantum gate $\exp(-\frac{iH_0t_0}{2^{u+v}})$. We denote this subroutine as $G(l-k_l+1)$. (b) The overall circuit as a cascade of the subroutines $G(l-k_l+1)$. (c) Implementation of $e^{iH_0\frac{t}{2^m}}$ in register M. The (u, v) gate can be realized by letting $t = \frac{t_0}{2^{u+v-m}}$.

Hoffmann, Phys. Chem. Chem. Phys. **10**, 5388 (2008).

[9] A. Aspuru-Guzik, A. D. Dutoi, P. J. Love, and M. Head-Gordon, Science **379**, 1704 (2005).

[10] D. Lidar and H. Wang, Phys. Rev. E **59**, 2429 (1999).

[11] H. Wang, S. Ashhab, and F. Nori, Phys. Rev. E , arXiv:1108.5902.

[12] J. You and F. Nori, Nature **474**, 589 (2011).
[13] J. You and F. Nori, Phys. Today **58**, 42 (2005).
[14] I. Buluta and F. Nori, Science **326** (2009).
[15] J. Dowling, Nature **439**, 919 (2006).
[16] L. Veis and J. Pittner, J. Chem. Phys. **133** (2010).
[17] L. Veis, J. Visnak, T. Fleig, S. Knecht, T. Saue, L. Visscher, and J. Pittner, arXiv:1111.3490v1 (2011).
[18] A. W. Harrow, A. Hassidim, and S. Lloyd, Phys. Rev. Lett. **15**, 150502 (2009).
[19] A. Daskin and S. Kais, J. Chem. Phys. **134** (2011).
[20] A. Daskin and S. Kais, Mol. Phys. **109**, 761 (2011).
[21] D. W. Berry, G. Ahokas, R. Cleve, and B. C. Sanders, Communications in Mathematical Physics **270**, 359 (2007).
[22] V. V. Shende, S. S. Bullock, and I. L. Markov, IEEE Trans. on Computer-Aided Design **25**, 1000 (2006).
[23] A. M. Childs, Nature Phys. **5**, 861 (2009).